ROBUST TIMEKEEPING IN CIRCADIAN NETWORKS: FROM GENES TO CELLS

Neda Bagheri [*,1] **Stephanie R. Taylor** [**,1]
Kirsten Meeker [**] **Linda R. Petzold** [**]
Francis J. Doyle III [***,2]

[*] *Dept. of Electrical and Computer Engineering, University of California Santa Barbara 93106-9560, U.S.A.*
[**] *Dept. of Computer Science, University of California Santa Barbara 93106-5070, U.S.A.*
[***] *Dept. of Chemical Engineering, University of California Santa Barbara 93106-5080, U.S.A.*

Abstract: Systems theoretic tools, including mathematical modeling, control theoretic analysis, and feedback design, advance the understanding of the circadian clock: a set of noisy oscillators that communicate to ensure its function as a reliable pacemaker. The clock's internal time, or *phase*, is a key performance measure used to investigate dynamics of a single deterministic oscillator for the purpose of generating insight into the behavior of coupled stochastic oscillators. The analysis of a single oscillator identifies appropriate coupling mechanisms for an ensemble of stochastic oscillators. Phase also serves as a critical control objective for a model predictive control algorithm that aims to correct mismatch between the biological clock and its environment.

Keywords: Phase dynamics, circadian rhythms, analysis, control, performance.

1. INTRODUCTION

Biological systems are characterized by complex dynamics. Undergirding a system's function are networks of interacting components (Sontag, 2004). To elucidate the mechanisms employed by these networks, biological experimentation and intuition are by themselves insufficient (Kitano, 2002). In the field of systems biology, investigators formalize the dynamical interactions as mathematical models and subject these models to systems theoretical analyses, with the goal of guiding further experimentation and increased understanding (Fall *et al.*, 2005). A perfect example of biological complexity is the circadian clock, which coordinates daily physiological behaviors of organisms across the kingdoms of life.

The mammalian circadian master clock resides in the suprachiasmatic nucleus (SCN), located in the hypothalamus (Reppert and Weaver, 2002). It is a network of multiple autonomous noisy oscillators, which communicate via neuropeptides to synchronize and form a coherent oscillator (Herzog *et al.*, 2004; Liu *et al.*, 2007). This coherent oscillator then coordinates the timing of daily behaviors, such as the sleep/wake cycle. Left in constant conditions, the clock will free-run with a period

[1] N.B. and S.R.T. contributed equally to this work.
We thank H. Mirsky and P. Chang for insightful comments.
[2] Corresponding author: frank.doyle@icb.ucsb.edu.
This project was supported in part by The Institute for Collaborative Biotechnologies, DAAD19-03-D-0004; NIH, GM078993; IGERT NSF, DGE02-21715; The Research Participation Program between the US DOE and AFRL/HEP.

of only *approximately* 24 hours and its internal time, or *phase*, will drift away from that of its environment. Thus, vital to a circadian clock is its ability to entrain to external time through environmental factors (Boulos *et al.*, 2002; Dunlap *et al.*, 2004; Daan and Pittendrigh, 1976*a*). To study the timekeeping abilities of the circadian clock, we employ a systems biology approach. Mathematical models are used in two complementary investigations, one involving the network of coupled oscillators, and the other involving the single coherent oscillator. In both cases we investigate the phase response behavior.

Proper phase response behavior is critical for synchronization both to environmental factors such as light, temperature, nutrition intake, and social interaction (Boulos *et al.*, 2002; Dunlap *et al.*, 2004; Daan and Pittendrigh, 1976*a*), and to other oscillators via intercellular signals such as vasoactive intestinal polypeptide (VIP) (Herzog *et al.*, 2004; To *et al.*, 2007). To study this behavior, phase response curves (PRCs) are collected. By mapping the arrival time of a stimulus to its resulting phase shift (advance or delay), the PRC characterizes the clock's time-dependent sensitivity to the given stimulus. In experimental settings, the best-studied factor is light (Daan and Pittendrigh, 1976*b*; Johnson, 1999; Winfree, 2001). Light PRCs have been used extensively to predict and better understand how biological oscillators are entrained by light input (Johnson, 1999; Johnson *et al.*, 2003; Comas *et al.*, 2006). A similar analysis is extended to mathematical models.

Commonly, circadian clocks are modeled with ordinary differential equations (ODEs) as single, deterministic limit cycle oscillators (Leloup and Goldbeter, 2003; Forger and Peskin, 2003). These models are used to reverse-engineer both the internal composition (transcriptional feedback loops) of the clock and the process of entrainment by light/dark cycles (Johnson *et al.*, 2003; Geier *et al.*, 2005). To capture the variability observed in biological data, additional models introduce stochasticity, via multiplicative noise in stochastic differential equations (SDEs) (Ueda *et al.*, 2002) or via a transformation from the differential equation setting to a discrete stochastic setting (Forger and Peskin, 2005; Gonze and Goldbeter, 2006). To capture the network behavior, spontaneous synchronization of coupled oscillators is modeled for the mammal and fly in (Ueda *et al.*, 2002; Gonze *et al.*, 2005; To *et al.*, 2007).

Synchronization and entrainment are critical phenomena of the circadian network that dictate an organism's level of performance. To further our understanding of such processes, we use ODEs, SDEs, and a discrete stochastic model in both the network and single-cell setting. In Section 2 we analyze synchronization of neurons in an SDE model by studying the phase response behavior of a single, deterministic cell. In Section 3 we define a population of neurons through a discrete stochastic model where the challenges associated with achieving synchronization are addressed via the study of a single oscillator. Section 4 describes a strategy for correcting the phase mismatch that arises when there is a difference between internal and external time.

2. ANALYSIS OF AND PREDICTIONS FOR COUPLED OSCILLATORS

We analyze the phase behavior of an SDE model of 100 coupled neurons in the *Drosophila melanogaster* circadian pacemaker (Ueda *et al.*, 2002). In an investigation of potential coupling mechanisms, Ueda *et al.* have developed a framework in which there are 960 potential coupling mechanisms. Each coupling mechanism is constructed such that each cell contains a component that sends a signal which is received by its neighbor cells. The signal then modulates a given target parameter. The authors show that a subset of the target/signal pairs produce spontaneous (in phase) synchronization among the cells. They discuss this phenomenon in terms of "day" and "night" systems, in which the mutual entrainment occurs in a manner similar to light (or dark) pulse entrainment.

We expand upon their analyses by modeling all 960 signal/target pairs. Of the 960, there are 84 that produce (in phase) synchrony. However, not all synchronizing mechanisms produce the same behavior. Notably, the period of oscillation is different for each target/signal pair, with values ranging from 20 hours to 37 hours. Because we are interested in rhythms that are circadian, we consider only those pairs that produce periods in the range of 20 to 28 hours. We examine the relationship between the signal/target pair and the resultant period of the synchronized system using a combination of numerical experimentation and mathematical analysis with an infinitesimal analog to the PRC. This is a step in pursuit of the fundamental question: What causes these coupling mechanisms to bring about synchronization while the others fail? Understanding the transition from asynchrony to synchrony is a significantly more complicated endeavor; thus, we focus on a synchronized system.

2.1 Methods

We simulate the SDE system for the 82 signal/target pairs that cause synchrony with a "circadian" period. The data describe *what* will

happen, but leave unanswered questions such as: *Why* are some signal/target pairs speeding up the oscillations and some slowing them down? *How* would an adjustment of the relative timing between the signal and the cell's phase change the timing? There is a rich literature concerning the mathematical analysis of coupled oscillators (Kuramoto, 1984; Hoppensteadt and Izhikevich, 1997; Winfree, 2001; Brown *et al.*, 2004). The most heavily studied systems, such as the Kuramoto model, assume either that interactions among oscillators are sinusoidal (Kuramoto, 1984; Strogatz, 2000) or that they perturb state velocities directly (Brown *et al.*, 2004). In circadian clock models, a signal sent to an oscillator ultimately manifests as the manipulation of a single parameter. Thus, to study the effects of signaling on the phase behavior, we must examine the effects of parametric manipulation on phase behavior. This motivated us to develop the parametric impulse phase response curve (pIPRC) in (Taylor *et al.*, 2007), which predicts the oscillator's velocity change in response to parametric perturbation. In the present work, we demonstrate its utility as a complement to numerical experimentation.

To utilize the pIPRC, we are compelled to investigate a deterministic model. Thus, we study a single neuron, modeled as a set of ODEs with a stable attracting limit cycle, e.g. $\dot{\mathbf{x}}(t) = \mathbf{f}(\mathbf{x}(t), \mathbf{p})$. The solution along the limit cycle is periodic with period τ, and we describe its progress along the cycle by its internal time, or *phase*, ϕ. When the clock is unperturbed, the phase progresses at the same rate as time, i.e., $d\phi(\mathbf{x}(t, \mathbf{p}))/dt \equiv 1$. When the clock is perturbed the velocity response is predicted by the pIPRC, i.e.

$$\mathbf{pIPRC}(\phi) = \frac{d}{dt}\frac{\partial \phi}{\partial \mathbf{p}}(t).$$

Consider a signal $\Delta p_j(t, \phi)$ which is a function either of time or phase. This signal will change the oscillator's velocity according to $\Delta\phi/\Delta t \approx \text{pIPRC}_j(\phi)\Delta p_j(t, \phi)$. Another interpretation is that for a pulse of duration Δt, a phase shift is incurred according to $\Delta\phi \approx \text{pIPRC}_j(\phi)\Delta p_j(t, \phi)\Delta t$. Using this interpretation, the pIPRC is a predictor for the PRC – the pIPRC characterizes the timing behavior of an oscillator alone while the PRC describes the response to a particular signal. To understand the period of the synchronized cells of the *Drosophila* clock, we study the relationship between the signal and the pIPRC for the target.

We must acquire the signal. To begin, we capitalize on the stable synchrony – in a synchronized system, each neuron sends the same signal at the same time. Thus, we mimic the intercellular signaling simply by assuming that all signals match that of a *single* neuron. The trace of the signal is acquired by simulating one cell as it sends the signal (without allowing the signal to feed back onto the cell). Two example signals along with the pIPRCs corresponding to their targets are shown in Fig. 2.

Before we begin our analysis, we evaluate the predictive power of the single cell model and of the pIPRC for each signal/target pair. First, we predict the period of the synchronized SDE population by simulating the ODE model, allowing it to signal itself. After several cycles it converges to a new limit cycle with a new period – the period of the synchronized system. In Fig. 1 we plot our prediction for the new period against the observed period of the SDE model of the full population. The square of the Pearson correlation coefficient, R^2, is 0.91 and the data is located within an hour of the observed values. Second, we use the pIPRC directly to make similar predictions. By treating ϕ as the independent variable (instead of time), we predict the change in period by assessing the effect of the signal on the oscillator over a single cycle. Integrating over the cycle,

$$\Delta\tau \approx -\int_0^\tau \text{pIPRC}_j(\phi)\Delta p_j(\phi)\, d\phi,$$

we find that the predictions are qualitatively accurate. Fig. 1 shows the predicted period change of the synchronized system versus the observed period change of the synchronized system. The R^2 value between observed and predicted periods is 0.65. The data are more scattered than those from the full-cell simulation, though the majority are within 1 hour of perfect prediction. We conclude that although neither of these methods are perfect predictors, their qualitative correctness supports our approach.

2.2 Analysis

Fig. 2 contains the traces of two signal/target pairs. Fig. 2(a) shows the relationship for a pair that causes the system to slow down. In this case, the target reaction rate is the maximal rate of degradation for clock component *tim* mRNA. The signal arrives at the tail end of the advance zone, and is active during the deadzone and the first half of the delay zone, leading to a cycle that is slower than nominal. Fig. 2(b) shows a pair for which the target reaction rate is the maximal rate of *clk* mRNA degradation. Here, the pIPRC shows nearly negligible delay regions. It follows that, regardless of the phase relationship between the signal and target, the oscillator will respond by speeding up.

In both of these cases, and in all cases that produce synchrony, the relationship between the

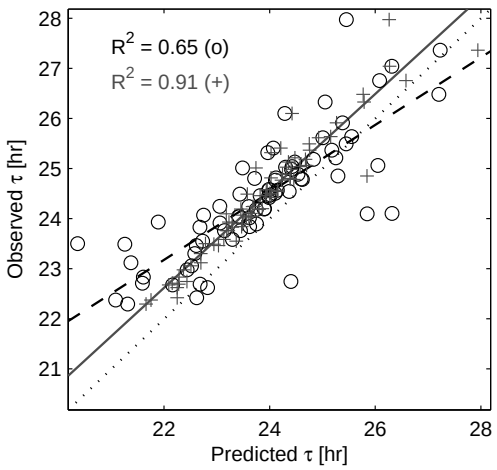

Fig. 1. Observed vs. Predicted Periods. For each signal/target pair that produces synchrony there is a black circle and a gray plus. The x-axis position indicates the period predicted using the pIPRC (circles) or using a single cell, signaling itself (pluses). For both data, the y-axis position indicates the period observed once collection of noisy cells becomes (and remains) synchronized. Perfect predictions fall on the dotted line. The dashed and solid lines represent the best fit by linear regression analysis, with $R^2 = 0.65$ for the pIPRC-predicted data and $R^2 = 0.91$ for the single-cell data.

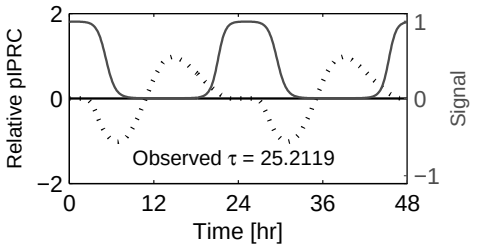

(a) Signal/Target Pair Producing Slow Oscillations

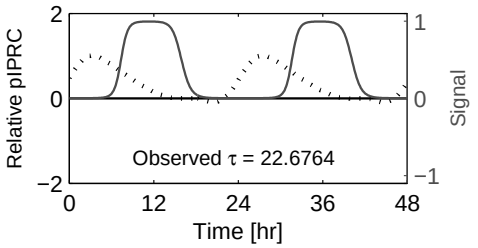

(b) Signal/Target Pair Producing Fast Oscillations

Fig. 2. Shown are the pIPRC (black dotted line) and signal trace (gray solid line) pairs that cause the coupled SDE system to synchronize with (a) long and (b) short periods. All curves are relative to the target parameter's nominal value; i.e., each signal represents fractional changes in the target parameter's value and each pIPRC predicts the velocity response to fractional changes.

signal and target meets the criteria for stable entrainment (data not shown). If the signal arrives early (because the phase of the system is a little behind), the system is sped up more (or slowed down less) than usual, and vice versa. The study of the pIPRC and signal is consistent with the observed behavior – the mutual entrainment is stable and the system remains synchronized. However, meeting the conditions for mutual entrainment is only a *necessary* factor; pairs arise that meet the requirements for stable entrainment but do not yield a transition to synchrony (data not shown). Figure 2(a) makes clear that a leftward signal shift of several hours produces a greater overlap of the advance region, meets the conditions for stable entrainment, and shortens the synchronized period. Thus, an understanding of the phase response behavior is key to unraveling the mechanisms *in vivo*.

3. STOCHASTIC MODEL OF COUPLED MAMMALIAN CIRCADIAN NEURONS

Phase response analysis is an important tool used to predict the coupling mechanism used by the mammalian clock. Evidence suggests that neurons in the SCN are synchronized via the neuropeptide VIP (Herzog *et al.*, 2004). VIP levels are high during the subjective day, and preliminary results show that VIP signals cause light-like phase shifts. Thus, the VIP signal is similar to the light signal, and the VIP target is similar to the light target. Data show that both VIP and light induce *Per* transcription (Piggins *et al.*, 1995), and it is predicted that the target of VIP signaling is *Per* transcription. Using this evidence, the authors of (Hao *et al.*, 2006; To *et al.*, 2007) model postulated mechanisms in which VIP signals are received by a cell through signal cascades culminating in the modulation of the parameter associated with *Per* transcription. Using an ODE model, To *et al.* incorporate this coupling mechanism into a population of non-identical cells, each of which is based on the gene regulatory network model of (Leloup and Goldbeter, 2003). They simulate scenarios in which (1) no coupling is present (and the cells drift out phase) and (2) coupling is present (and the cells form a coherent oscillator), thus demonstrating that their mechanism is capable of creating the spontaneous synchronization seen in the data.

Biological experiments show that uncoupled neurons are either damped or sloppy oscillators (Aton *et al.*, 2005). The periods of isolated neurons show both a broad distribution of periods and temporal (cycle-to-cycle) variability (Herzog *et al.*, 2004). The model presented in (To *et al.*, 2007) shows a broad distribution of periods across cells, but

none of the cycle-to-cycle variability. To introduce that variability, we develop a stochastic model that builds on these efforts, adding the intrinsic noise due to the discrete nature of reactions in the SCN neuron. The present model employs a 2-dimensional grid of 9 SCN neurons and is the discrete stochastic version of the model in (Leloup and Goldbeter, 2003) with the coupling mechanism from (To *et al.*, 2007). Preliminary results, synchronizing a small number of coupled cells, support the validity of the mechanism in the presence of noise. For a more detailed description of the signaling mechanism, see Equations 1-7 and Table 1 in the model supplement of (To *et al.*, 2007).

3.1 Discrete Stochastic Simulation

The stochastic simulation algorithm (SSA) (Gillespie, 1976; Gillespie, 1977) generates exact trajectories of the populations of chemical species, given a description of the reaction system consisting of the stoichiometric matrix, ν_{ij}, and the propensity functions a_j. The probability density function $P(x,t|x_0,t_0)$ is defined as the probability the system will be in state x at time t, given that it was in state x_0 at time t_0. The time evolution of $P(x,t|x_0,t_0)$ is described by the chemical master equation,

$$\frac{\partial P(x,t|x_0,t_0)}{\partial t} = \sum_{j=1}^{M}[\ a_j(x-\nu_j) P(x-\nu_j,t|x_0,t_0) - a_j(x)P(x,t|x_0,t_0)]. \quad (1)$$

The stoichiometric matrix ν_{ij} describes how the populations of species change with each reaction and has dimensions of number of species $i = 1,\cdots,N$ by number of reactions $j = 1,\cdots,M$. The propensity function a_j predicts the probability of each reaction occurring during the next infinitesimal time interval, given the current species populations. We use StochKit (StochKit, 2007) package, a stochastic simulation tool developed at University of California, Santa Barbara, to simulate the two dimensional grid of neurons using the SSA.

3.2 Oscillatory Range of Per Transcription Rate

The introduction of noise alters the behavior of the single cells such that additional tuning is required to achieve synchrony. In particular, because VIP signaling ultimately manifests as modulation of the rate of *Per* transcription, special attention must be paid to the levels of *Per* mRNA and its rate of transcription, $\nu_{sP}(t)$. The basal rate, ν_{sP0}, characterizes the behavior of an isolated cell. *Per* mRNA for several ν_{sP0} are shown in Fig. 3. The depletion or accumulation of *per* mRNA that occurs when ν_{sP0} is below 1.2 or above 1.8 indicates that we have upset the balance between (1) the transcription rate and (2) the combination of the transport (from nucleus to cytoplasm) and degradation. The current model normalizes the coupling for the size of the grid, but does not maintain the median of $\nu_{sP}(t)$ as coupling is added. For the coupled population to exhibit synchrony, we have observed that the median value of $\nu_{sP}(t)$ must stay within the range that produces oscillations in an individual cell. Thus, to achieve synchrony, the basal transcription rate ν_{sP0} is decreased to 1.0 for the coupling weight used in the present work. This produces a median *per* mRNA population comparable to the uncoupled case with $\nu_{sP0} = 1.5$. At this basal transcription rate, all isolated cells are damped oscillators. To better match the biological observation that many isolated cells show sustained oscillations, it is necessary either to weaken the coupling or to adjust the transport or degradation rate to re-balance the *per* mRNA level.

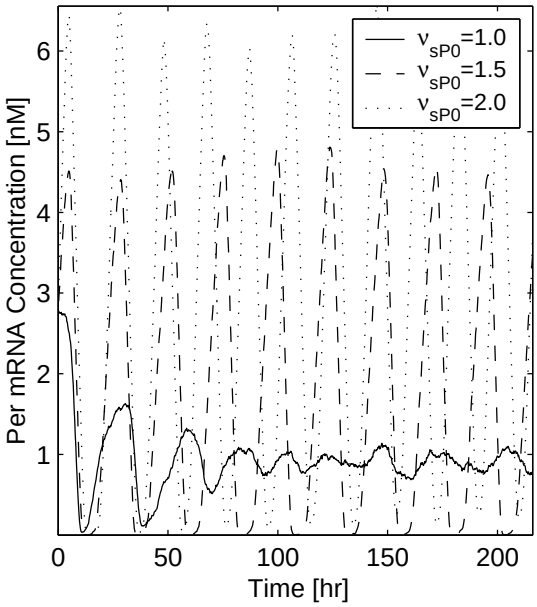

Fig. 3. *Per* mRNA concentration as a function of basal transcription rate ν_{sP0} in uncoupled cells. For ν_{sP0} below 1.2 *per* mRNA concentrations exhibit damped oscillations for the ten day period simulated. For ν_{sP0} above 1.8 *per* mRNA concentrations begin to grow in amplitude with minima greater than zero.

3.3 Discrete Stochastic Simulation

The results of a single simulation trajectory of a 3x3 grid of coupled cells are shown in Fig. 4(a) and

Fig. 4(b). The radius $r(t)$ of the complex order parameter

$$re^{i\Psi} = \frac{1}{N}\sum_{j=1}^{N} e^{i\theta_j} \tag{2}$$

measures the phase coherence of the collective rhythm of N coupled oscillators (Strogatz, 2000). If the oscillators are in phase, then $r \approx 1$. θ_j are the phase of each oscillator and $\Psi(t)$ is the average phase. The increase in $r(t)$ from 0.6 to 0.8 in one cycle is comparable to the results from (To *et al.*, 2007), where a deterministic model with normal distribution of some of the parameters was used to create a grid of coupled heterogeneous cells.

The difference in peak amplitudes in Fig. 4(a) is due to the small grid and the effect of its boundaries. The discrete stochastic simulation of larger grids is a goal of this research and will require improvements in code performance. Reproducing the period and cycle-to-cycle variability of uncoupled single neurons will require increasing the effective noise level by lowering the volume. This study, done at a high volume, demonstrates a method for balancing the coupling strength that will produce phase coherence with a basal *Per* transcription rate that will sustain oscillations.

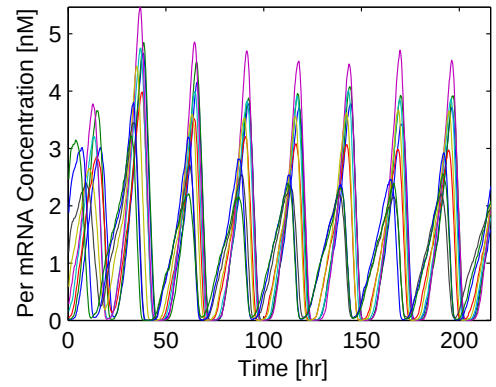

(a) *Per* mRNA in Coupled 3x3 Grid

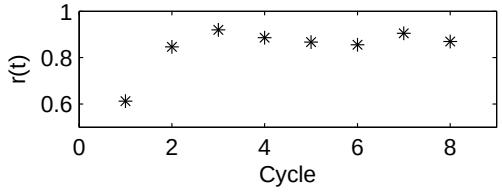

(b) Complex Order Parameter Radius for 3x3 Coupled Grid

Fig. 4. For a single SSA simulation of a 3x3 grid of coupled cells (with $\Omega = 2000$), we show (a) the trajectory of *Per* mRNA concentration over time, and (b) its degree of phase coherence.

4. PHASE AS A CONTROL OBJECTIVE

As signaling among a network of cells serves to synchronize the phase of the individuals, signaling from the environment serves to entrain the phase of the emergent coherent oscillator. Thus, the light signal received by an organism induces phase shifts that calibrate its internal phase to external time. In this section the clock is regarded as a single deterministic oscillator and we apply a model predictive control (MPC) algorithm as a tool to minimize the phase difference between the organism and the environment.

In the early 1970's, Daan and Pittendrigh investigated light-induced phase shifts in free-running organisms through the development of phase response curves. Watanabe *et al.* (2001) build upon Daan and Pittendrigh's investigation of light-induced phase shifts in free-running organisms by proving that the basis for phase entrainment in mammals involves both advance and delay components of the phase response curve . Boulos *et al.* (2002) extend the investigation/application of phase response curves by establishing bright light treatment as a means to accelerate circadian re-synchronization rates. In a previous study, a closed-loop model predictive control algorithm that relies on an evolutionary strategy to determine an optimal sequence of light pulses is used to reset the organisms' phase (Bagheri *et al.*, 2007). In this study the optimal sequence of light inputs is determined as a function of MPC tuning parameters as well as the attributes of the driving force (light).

4.1 A Mammalian Model

A detailed model that describes circadian dynamics of a single mammalian cell through 61 ODEs serves as the example system (Forger and Peskin, 2003; Mirsky *et al.*, 2007). It may be generally defined as a set of nonlinear ordinary differential equations where t is continuous in time, $\mathbf{x}(t)$ defines the n-length state vector, $L(t)$ defines the environmental light input, $u(t)$ defines the controlled light input, and $\mathbf{f}(\mathbf{x}(t), L(t), u(t))$ defines the n-length system dynamics:

$$\begin{aligned} \dot{\mathbf{x}}(t) &= \mathbf{f}\left(\mathbf{x}(t), L(t), u(t)\right), \\ \mathbf{x}(t_0) &= \mathbf{x}(0), \end{aligned} \tag{3}$$

where $\mathbf{x}(t) \in \Re^{n\times 1}$, $L(t)$, and $u(t) \in \Re^{1\times 1}$. Once the asymptotically stable nonlinear oscillator converges to a limit cycle, it exhibits a period τ: $\mathbf{x}(t+\tau) = \mathbf{x}(t)$. In this paper, the nominal model (a version of the model that has converged to the natural light/dark environment where $u(t) = 0$

and $L(t)$ oscillates as a square wave between values 3.39E-2 and 0) is used to define the reference trajectory, $\mathbf{r}(t)$. A circadian time of 0 reflects dawn while a circadian time of 12 reflects dusk, assuming regular 24 hour day:night cycles.

4.2 MPC of Light Pulses

A model predictive control strategy (Henson and Seborg, 1997; Morari and Lee, 1999) is used to increase the re-synchronization rate of circadian oscillators through the systematic addition of light. The control algorithm steps through state trajectories at t_s-hour intervals, where k serves as the discrete time index reflecting the current simulation time t evaluated at t_s intervals. In this work, the time step and duration of the manipulated control variable, light, are equivalent.

The manipulated light profile, $u(t)$, optimizes an open-loop performance objective on a time interval extending from the current time to the current time plus a prediction horizon, $P = 54$hr, allowing the algorithm to take control action at the current time in response to a forecasted error. The move horizon limits the number of controlled light pulses within the prediction horizon; $M =$ 3hr. Beyond M hours of simulation, the predicted model defaults to $u(t) = 0$. Future behaviors for a variety of control inputs are computed according to a model of the plant.

The algorithm chooses a series of control inputs by minimizing a performance criterion over a future horizon. Once the most fit control sequence, $\mathbf{u}^* \in \Re^{M/t_s \times 1}$, only the first control, $\mathbf{u}^*(1)$, is implemented. Feedback is incorporated by using the next measurement to update the optimization problem for the next time step.

Assuming $u_{min}(t)$ =-3.39E-2, $u_{max}(t)$ =3.39E-2, and $L(k) + u(k) \geq 0$, the performance function penalizes the normalized predicted error between the reference and controlled trajectories, $\mathbf{e}(k)$, and its corresponding control sequence, $\mathbf{u}(k)$. To avoid penalizing transient effects, the state error is weighted uniformly over the move horizon and with increasing weight of slope 2 over the prediction horizon (via $\mathbf{Q}$). The cost of applying a light input is always weighted uniformly (via $\mathbf{R}$). The cost of implementing an M-length control input $\mathbf{u}(\cdot)$ beginning at time k that minimizes the error over P hours is defined as

$$J = \min_{\mathbf{u}(\cdot)} \left[(\mathbf{eQ})^T (\mathbf{eQ}) + (\bar{\mathbf{u}}\mathbf{R})^T (\bar{\mathbf{u}}\mathbf{R}) \right]. \quad (4)$$

Once the controlled state trajectories converge to within 15% of the corresponding nominal (or reference) state trajectories, the system is considered to be in phase: $T_r = \min_k [|e(k)|_\infty \leq 0.15]$. For further details concerning the MPC algorithm, please refer to (Bagheri *et al.*, 2007).

4.3 MPC Tuning Parameters

The optimum control sequence, $\mathbf{u}^*$, is determined by enumerating the solutions over a grid in the solution space (light magnitude as a function of time). The algorithm approaches a globally optimal solution as the total possible quantization steps of the control input and computational expense increase. The efficacy of the algorithm is tested with respect to a quantization step of 2, 4, 8, and 16 steps (Fig. 5(a)). Results suggest that the decrease in phase recovery time may not outweigh the increase in computation time. The phase resetting dynamics of a control input with 2 and 8 possible steps are investigated below.

Similarly, the efficacy of the algorithm is tested with respect to a control input of duration 1, 2, and 3 hours (reflecting a move horizon of 3, 6, and 9-hours, respectively) (Fig. 5(b)). Results suggest that although shorter light pulses offer a more dynamic manipulated variable profile, it shortens the move horizon and may reduce the utility of model predictive control. Conversely, while longer light pulses offer a longer move horizon, it may reduce the possible control profiles since longer light pulses eventually lead to arrhythmic behavior (Ohta *et al.*, 2005). In the remainder of this study, the duration of control is set to 2 hours.

4.4 Results

The nonlinear properties of biological oscillators often cause different phase-resetting dynamics with respect to the initial condition, IC, and initial phase difference, IP. The initial condition describes the time at which the organism settles into the new environment and begins entrainment; the initial phase difference describes the number of time zones bypassed upon arrival. Hence, phase recovery times are described as a function of both the IC and IP.

We generate phase recovery dynamics for three different simulation schemes: (1) The open-loop algorithm where environmental light/dark cycles entrain the system, (2) the closed-loop MPC algorithm where the manipulated control variable (light) has two possible values, and (3) where the manipulated control variable has eight possible values. Phase recovery times may be consolidated into a 3-dimensional diagram (Fig. 6) where the recovery times are plotted with respect to both initial phase differences and initial conditions. As such, we may better visualize the nonlinear dynamic behavior of phase resetting. Although

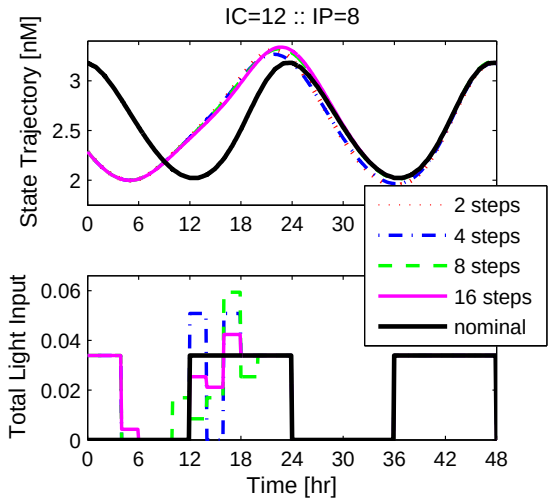

(a) Control Input Quantization

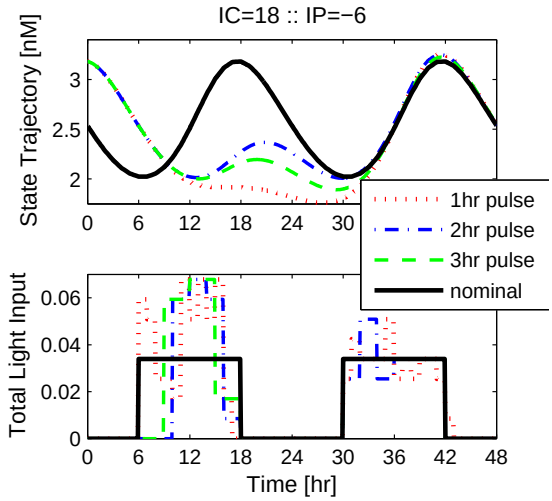

(b) Duration of Control

Fig. 5. (a) The recovery time associated with a control input that allows 2, 4, 8, and 16 possible values is 36.8, 35.6, 34.7, and 34.6-hours respectively. (b) The recovery time associated with a 1, 2, and 3-hour control input is 36.7, 34.7, and 35.2-hours respectively. Top subplots depict state dynamics as they recover from an (a) 8 hour or (b) -6 hour initial phase difference and converge to the reference trajectory (depicted by the bold solid line). Lower subplot depict the associated control moves that begin to take action at a circadian time of (a) 12 hours or (b) 18 hours, where the bold solid square wave describes environmental (nominal) light/dark cycles.

the closed-loop algorithm significantly increases re-synchronization rates, using 2 possible control values is often just as effective as using 8 – the flexibility of control inputs does not affect its efficacy.

The open-loop environmental control strategy requires (at most) 64.7 hours to synchronize a ±12-hour initial phase difference beginning at an initial condition of 12-hours (Table 1) (Bagheri *et*

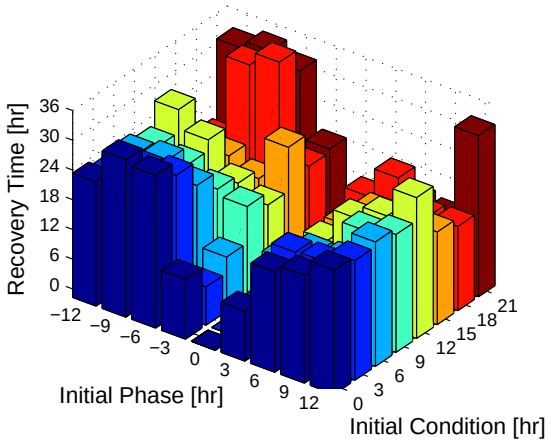

(a) 2-Step Closed-Loop Control

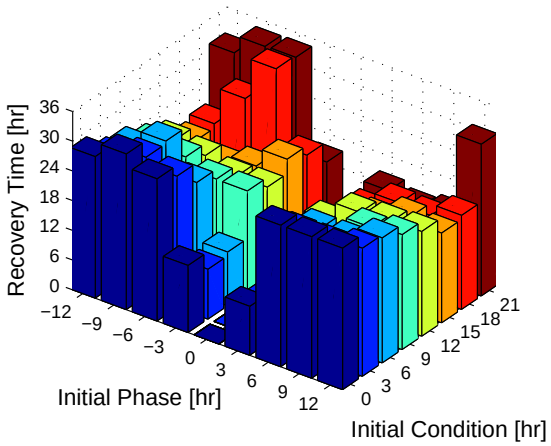

(b) 8-Step Closed-Loop Control

Fig. 6. Recovery time with respect to IC and IP. The time required to reset the system's phase is reflected on the vertical axis. The shade of each bar is consistent along the IC. Although the closed-loop algorithms significantly improve upon open-loop phase-resetting times, IC=12hr is one of the few data sets that improves with the increase of control steps.

al., 2007). The closed-loop 2-step algorithm (Fig. 6(a)) improves upon the maximum recovery time as it requires only 36.8 hours to recover a -6-hour initial phase difference (at IC=18hr). Surprisingly, the 8-step algorithm does not significantly improve phase resetting as it requires 34.7 hours to recover the same conditions. For this reason, a 2-step algorithm (which requires 0.17 hours of computation time per simulation) is more applicable/efficient for use in applications – such as light therapy – when compared to the 8-step algorithm (which requires 3.5 hours of computation per simulation).

We improve phase-resetting performance via implementation of a closed-loop model predictive

Table 1. Maximum recovery times with respect to the set of initial conditions for open- and closed-loop algorithms. The bold-face recovery times relate to the overall maximum recovery for over the entire set.

	Open-Loop		**2-Step Algorithm**		**8-Step Algorithm**	
IC	Recovery	IP	Recovery	IP	Recovery	IP
0 hr	32.50 hr	-6 hr	31.80 hr	-9 hr	31.40 hr	-9 hr
3 hr	31.40 hr	-9 hr	28.00 hr	-6 hr	28.10 hr	-9 hr
6 hr	47.50 hr	-9 hr	26.00 hr	-9 hr	28.60 hr	-9 hr
9 hr	46.90 hr	±12 hr	23.80 hr	±12 hr	23.20 hr	±12 hr
12 hr	**64.70 hr**	±12 hr	28.40 hr	±12 hr	21.10 hr	±12 hr
15 hr	61.70 hr	±12 hr	24.70 hr	-3 hr	21.50 hr	-3 hr
18 hr	40.80 hr	6 hr	**36.80 hr**	-6 hr	**34.70 hr**	-6 hr
21 hr	35.50 hr	-6 hr	34.00 hr	-9 hr	34.30 hr	-6 hr

control algorithm. This evidence supports the hypothesis that, in general, open-loop light/dark cycles are not optimized to reset large phase differences (Bagheri *et al.*, 2007). Instead, organisms may have evolved to efficiently reset small phase differences since rapid transit across multiple time zones is a recent innovation.

5. CONCLUSION

In this work, we develop and apply systems theoretic tools for the investigation of circadian phase properties as single deterministic, and populations of stochastic models. The study of synchronization supports the reverse-engineering of the clock in the SCN while providing a foundation upon which to engineer other communication networks. Analysis of the pIPRC provides separation of the timing characteristics of the oscillator and signal. Altering the signal (via a change in duration, magnitude, or overall shape) can have profound affects, and these effects are prescribed by the pIPRC. For example, it is possible to speed up an oscillator when (and only when) there is an advance area in the target pIPRC. To synchronize, the signal must meet the conditions for stable entrainment.

Investigating phase dynamics of circadian oscillators also provides a forum to address resynchronization properties of the clock. Control theoretic tools bring novel insights for unraveling the design principles of the circadian clock, and further, point to opportunities for therapeutic approaches to resetting the clock. The application of a closed-loop model predictive control algorithm provides a sequence of light pulses that force the circadian system to recover phase differences at a fraction of the natural open-loop simulated mammalian recovery time.

REFERENCES

Aton, S.J., C.S. Colwell, A.J. Harmar, J. Waschek and E.D. Herzog (2005). Vasoactive intestinal polypeptide mediates circadian rhythmicity and synchrony in mammalian clock neurons. *Nat. Neurosci.* **8**(4), 476–483.

Bagheri, N., J. Stelling and F.J. Doyle III (2007). Circadian phase entrainment via nonlinear model predictive control. *Int. J. Robust Nonlinear Control.* submitted.

Boulos, Z., M.M. Macchi, M.P. Stürchler, K.T. Stewart, G.C. Brainard, A. Suhner, G. Wallace and R. Steffen (2002). Light visor treatment for jet lag after westward travel across six time zones. *Aviat. Space Environ. Med.* **73**, 953–963.

Brown, E., J. Moehlis and P. Holmes (2004). On the phase reduction and response dynamics of neural oscillator populations. *Neural Comput.* **16**(4), 673–715.

Comas, M., D. G M Beersma, K. Spoelstra and S. Daan (2006). Phase and period responses of the circadian system of mice (Mus musculus) to light stimuli of different duration. *J. Biol. Rhythm.* **21**(5), 362–372.

Daan, S. and C.S. Pittendrigh (1976*a*). A functional analysis of circadian pacemakers in nocturnal rodents. I. The stability and lability of spontaneous frequency. *J. Comp. Physiol.* **106**, 223–252.

Daan, S. and C.S. Pittendrigh (1976*b*). A functional analysis of circadian pacemakers in nocturnal rodents. II. The variability of phase response curves. *J. Comp. Physiol.* **106**, 253–266.

Dunlap, J.C., Loros, J.J. and DeCoursey, P.J., Eds. (2004). *Chronobiology: Biological Timekeeping.* Sinauer Associates, Inc.. Sunderland, MA.

Fall, C.P., E.S. Marland, J.M. Wagner and J.J. Tyson (2005). *Computational Cell Biology.* Springer. New York.

Forger, D.B. and C.S. Peskin (2003). A detailed predictive model of the mammalian circadian clock. *P. Natl. Acad. Sci. U S A* **100**(25), 14806–14811.

Forger, D.B. and C.S. Peskin (2005). Stochastic simulation of the mammalian circadian clock. *P. Natl. Acad. Sci. U S A* **102**(2), 321–324.

Geier, F., S. Becker-Weimann, A. Kramer and H. Herzel (2005). Entrainment in a model of the mammalian circadian oscillator. *J. Biol. Rhythm.* **20**(1), 83–93.

Gillespie, D.T. (1976). A general method for numerically simulating the stochastic time evolution of coupled chemical reactions. *J. Comput. Phys.* **22**(4), 403–434.

Gillespie, D.T. (1977). Exact stochastic simulation of coupled chemical reactions. *J. Phys. Chem.* **81**, 2340–2361.

Gonze, D. and A. Goldbeter (2006). Circadian rhythms and molecular noise. *Chaos* **16**(2), 026110.

Gonze, D., S. Bernard, C. Waltermann, A. Kramer and H. Herzel (2005). Spontaneous synchronization of coupled circadian oscillators. *Biophys. J.* **89**(1), 120–129.

Hao, H., D.E. Zak, T. Sauter, J. Schwaber and B.A. Ogunnaike (2006). Modeling the VPAC2-activated cAMP/PKA signaling pathway: from receptor to circadian clock gene induction. *Biophys. J.* **90**(5), 1560–1571.

Henson, M.A. and Seborg, D., Eds. (1997). *Nonlinear Process Control*. Prentice Hall. Upper Saddle River, NJ.

Herzog, E.D., S.J. Aton, R. Numano, Y. Sakaki and H. Tei (2004). Temporal precision in the mammalian circadian system: a reliable clock from less reliable neurons. *J. Biol. Rhythm.* **19**(1), 35–46.

Hoppensteadt, F.C. and E.M. Izhikevich (1997). *Weakly Connected Neural Networks*. Vol. 126 of *Applied Mathematical Sciences*. Springer-Verlag. New York.

Johnson, C.H. (1999). Forty years of PRCs–what have we learned?. *Chronobiol. Int.* **16**(6), 711–43.

Johnson, C.H., J.A. Elliott and R. Foster (2003). Entrainment of circadian programs. *Chronobiol. Int.* **20**(5), 741–774.

Kitano, H. (2002). Systems biology: a brief overview. *Science* **295**, 1662–1664.

Kuramoto, Y. (1984). *Chemical oscillations, waves, and turbulence*. Springer-Verlag. Berlin.

Leloup, J.-C. and A. Goldbeter (2003). Toward a detailed computational model for the mammalian circadian clock. *P. Natl. Acad. Sci. U S A* **100**(12), 7051–7056.

Liu, A.C., D.K. Welsh, C.H. Ko, H.G. Tran, E.E. Zhang, A.A. Priest, E.D. Buhr, O. Singer, K. Meeker, I.M. Verma, F.J. Doyle III, J.S. Takahashi and S.A. Kay (2007). Intercellular coupling confers robustness against mutations in the SCN circadian clock network. *Cell*. in press.

Mirsky, H., R. Gunawan, S.R. Taylor, J. Stelling and F.J. Doyle III (2007). Noise propagation and sensitivity in mammalian circadian clocks. *P. Natl. Acad. Sci. U S A*. submitted.

Morari, M. and J.H. Lee (1999). Model predictive control: Past, present and future. *Comput. Chem. Eng.* **23**, 667–682.

Ohta, Hidenobu, Shin Yamazaki and Douglas G McMahon (2005). Constant light desynchronizes mammalian clock neurons. *Nat. Neurosci.* **8**(3), 267–269.

Piggins, H.D., M.C. Antle and B. Rusak (1995). Neuropeptides phase shift the mammalian circadian pacemaker. *J. Neurosci.* **15**(8), 5612–5622.

Reppert, S.M. and D.R. Weaver (2002). Coordination of circadian timing in mammals. *Nature* **418**(6901), 935–941.

Sontag, E.D. (2004). Some new directions in control theory inspired by systems biology. *Syst. Biol. (Stevenage)* **1**(1), 9–18.

StochKit (2007). http://www.cs.ucsb.edu/∼cse/StochKit.

Strogatz, S.H. (2000). From Kuramoto to Crawford: exploring the onset of synchronization in populations of coupled oscillators. *Physica D* **143**, 1–20.

Taylor, S.R., R. Gunawan, L.R. Petzold and F.J. Doyle III (2007). Sensitivity measures for oscillating systems: Application to mammalian circadian gene network. *IEEE Trans. Circuits Syst. I*. submitted.

To, T.-L., M.A. Henson, E.D. Herzog and F.J. Doyle III (2007). A molecular model for intercellular synchronization in the mammalian circadian clock. *Biophys. J.* in press.

Ueda, H.R., K. Hirose and M. Iino (2002). Intercellular coupling mechanism for synchronized and noise-resistant circadian oscillators. *J. theor. Biol.* **216**(4), 501–512.

Watanabe, K., T. Deboer and J.H. Meijer (2001). Light-induced resetting of the circadian pacemaker: Quantitative analysis of transient versus steady-state phase shifts. *J. Biol. Rhythm.* **16**, 564–573.

Winfree, A.T. (2001). *The Geometry of Biological Time*. Springer. New York.